Analysis and Simulation of a Wideband Dual-Band Balanced-to-Unbalanced Gysel Power Divider Using Coupled Lines

Abdullah J. Alazemi* and Fatma H. Almesri

Department of Electrical Engineering, College of Engineering and Petroleum, Kuwait University, Kuwait.

** Corresponding Author: aalazem.ku@ku.edu.kw*

Submitted: 14-07-2022

Revised: 03-10-2022

Accepted: 11-10-2022

ABSTRACT

In this article, theoretical analysis and simulation of a wideband dual-band balanced to unbalanced Gysel power divider using coupled lines are proposed for dual-band WiFi applications. The proposed power divider consists of three coupled line sections, stepped-impedance stub, two grounded resistors, and a dual-band phase inverter. The dual-band phase inverter is used to perform the differential functionality at the input port. The use of the coupled lines results in a wide frequency range, compact size, flexible structure, and more freedom in choosing the design parameters. The closed-form equations and the ABCD matrix are derived using even and odd mode analysis and precise electrical design parameters are determined. The power divider was simulated at 2.4 GHz and 5 GHz, and great performance had been achieved; all ports are matched at the two frequencies with a 10-dB input fractional bandwidth of 45.83% at 2.4 GHz and 21.7% at 5 GHz. The isolation between output ports was more than 15 dB within the frequency bandwidth and the power was divided equally between output ports with the same phase. In addition, a perfect common mode suppression was reached, and the differential functionality was a success. Moreover, the device is simulated using Keysight-ADS and the results agreed well with the derived equations results. The device can be used for any application requiring dual-band WiFi connectivity.

Keywords: Dual-band; power divider; WiFi; Coupled lines; Balanced-to-unbalanced; Even-odd mode; ABCD matrix; Mixed mode.

INTRODUCTION

Power dividers or power splitters are passive microwave devices that usually splits an input signal into two or more equal output signals, and unequal power division between output signals is also possible. Moreover, power dividers may have any number of ports and because of the design symmetry, they can also be used as power combiners. Power handling, output isolation, and phase and port matching are required for these devices (Yoon and Kim, 2021; Alazemi and Kourah, 2019). Power dividers/combiners are commonly implemented in modern communication systems, RF, and microwave circuits.

Wilkinson and Gysel power dividers are examples of the most important and well-known power dividers. Lately, the need of enhancing the standards of the multi-band microwave components was necessary for the development of microwave circuits and wireless communications systems. Differential RF circuits are used instead of single ended circuits in modern communication systems because of their capability to immunize noise and electromagnetic interference since they can suppress common mode noise. Therefore, differential passive components like balanced filters (Wu et al., 2007; Lim et al., 2010), balanced couplers (Jiao et al., 2018; Li et al., 2019), diplexers (Lobato-Morales et al., 2012; Zhou et al., 2014), and balanced power dividers (Zhang et al. 2017; Yu and Sun, 2015) have been recently widely used in communication systems. Power dividers can be classified based on the type of differential input/output ports into four categories: unbalanced to unbalanced (UTU) (Sun et al., 2011; Wang et al., 2014), unbalanced to balanced (UTB) (Zhang et al. 2017; Wu et al., 2018), balanced to unbalanced (BTU) (Xu et al., 2015; Zhu et al., 2020), and balanced to balanced (BTB) (Wu et al., 2013; Xia et al., 2012; Li et al., 2018). Power dividers are implemented using various methods such as open and short stubs (Sun et al., 2011; Yoon and Kim, 2021), coupled lined and lumped resistors (Wang et al., 2014; Wang et al., 2013), and stepped impedance transmission lines (Yu and Sun, 2015).

Many recent works presented dual-band designs of differential power dividers which are highly required in contemporary communications systems with dual communications standards (Feng et al., 2019; Zhu et al., 2020; Zhuang et al., 2018; Liu et al., 2022). In dual-band receivers, dual-band balanced receiving antennas are typically used for the aforementioned advantages of differential devices. They are usually connected to other single-ended dual-band components using a combination of dual-band baluns and dual-band dividers. Recent works suggested a better alternative to this structure by using BTU dividers to combine the balun and the divider into one device and hence achieving size reduction. Zhu et al., 2020 proposed a dual-band BTU divider by introducing a dual-band phase inverter to a modified Gysel divider with a single isolation resistor. Another dual-band BTU divider was developed in (Zhuang et al., 2018) by replacing each line in a single-band BTU divider with a dual-band impedance transformer. A recent dual-band BTU divider was presented in (Liu et al., 2022) which used two layers of slotted circular patch resonators that are aperture-coupled. However, the dual-band BTU dividers in (Zhu et al., 2020; Zhuang et al., 2018; Liu et al., 2022) have some drawbacks related to their structures. The designs in (Zhu et al., 2020; Zhuang et al., 2018) are developed by replacing single-band components with their dual-band counterparts which tends to increase their size. Similarly, the design in (Liu et al., 2022) is of two-layered structure which is difficult to fabricate. Therefore, it is our aim in this article to design a dual-band BTU divider that has a compact and simple form. Such a design will be particularly useful in reducing the size of dual-band receivers which is one of the main motivations behind BTU dividers in the first place.

In this article, a wideband dual-band balanced to unbalanced (BTU) Gysel power divider designed using coupled lines is proposed for 2.4 and 5 GHz operating frequencies. The proposed device consists of three coupled line sections, a dual-band phase inverter, a stepped impedance stub, and two grounded resistors. With such a structure, a compact, simple, and flexible design is achieved with wideband dual-band capability. The proposed device is theoretically analyzed and is also simulated using Keysight's Advanced Design System (ADS). The simulated results demonstrate the excellent performance achieved by proposed device at both operating frequencies in terms of power division, common mode suppression, and output isolation.

The rest of the paper is organized as follows. First, the design and analysis of the proposed device are presented. In this section, the mixed mode S-parameters of the proposed device are derived using even- and odd-modes analysis. Also, the effect of the frequency ratio of the design's line impedances (and hence the size) is studied. Then, the results and discussion section is presented. In this section, the device is built and simulated in Keysight's Advanced Design System (ADS), and the results are demonstrated and show a great agreement with theoretical results. Finally, the paper is concluded.

DESIGN AND ANALYSIS

In this sections, the development of the proposed dual-band BTU divider is presented. First, a dual-band unbalanced Gysel power divider is presented, and it will be the core of the proposed device. By incorporating a dual-band phase inverter and a stepped-impedance stub, this core divider will be developed into the proposed dual-band BTU divider.

Core Dual-Band Unbalanced Divider

Fig. 1 shows the schematic of a dual-band unbalanced Gysel power divider. The device consists of three coupled line sections, a transmission line section, two grounded resistors, and an open stub. The ports have an internal resistor, which is commonly equal to 50 Ω. The circuit parameters are calculated as follow: $Z_1 = 55\ \Omega$, $Z_{e1} = 52\ \Omega$, $Z_{o1} = 40\ \Omega$, $Z_{e2} = 50\ \Omega$, $Z_{o2} = 32\ \Omega$, $Z_{e3} = 60.37\ \Omega$, $Z_{o3} = 50\ \Omega$, $Z_S = 80\ \Omega$, and $R_1 = R_2 = 54.9\ \Omega$ using the equations in (Wang et al., 2014). All transmission lines and stubs have the same length which is 58.4°.

Fig. 2 shows the simulated S-parameters of the power divider at operating frequencies (2.4 GHz & 5 GHz). Fig. 2a shows that all ports are matched ($|S_{11}|$, $|S_{22}|$, $|S_{33}|$ < -10 dB), the power is divided equally between ports 2 and 3 ($|S_{21}| = |S_{31}|$= -3 dB), the output signals are in phase ($|\phi_2| = |\phi_3| = 90^\circ$), and the output ports are isolated from each other ($|S_{23}|$, $|S_{32}|$ < -20 dB).

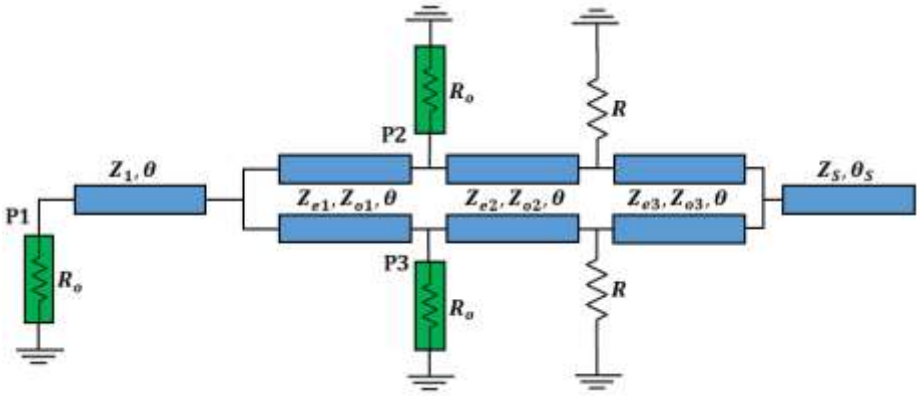

Figure 1. A schematic of a dual-band Gysel power divider using coupled lines.

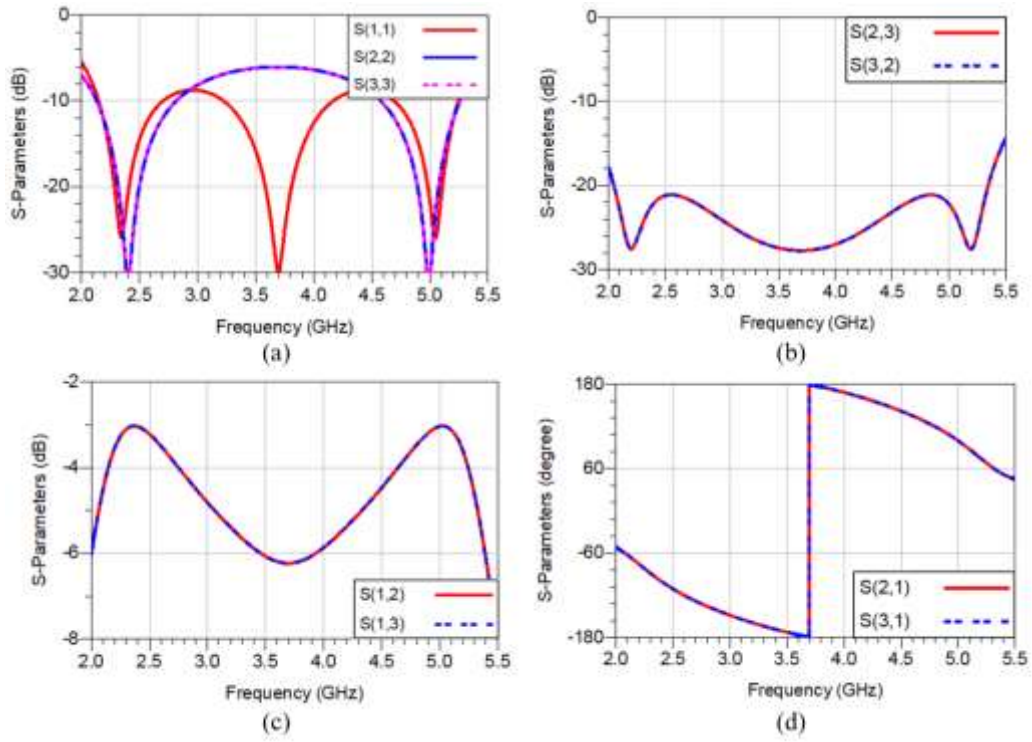

Figure 2. The simulated S-parameters of dual-band Gysel power divider using coupled lines: (a) The return loss at the input and output ports, (b) The isolation between output ports, (c) The insertion loss from port 1 to ports 2 or 3, (d) The phases of the insertion loss parameters.

Dual-Band Phase Inverter

An essential component to develop the divider in Fig. 2 into a BTU Gysel power divider is the dual-band phase inverter shown in Fig. 3. This inverter is equivalent to a line with impedance Z_1 and length 180° at both design frequencies. The structure parameters (impedances Z_a and Z_b; and lengths θ_a and θ_b defined at f_1) are calculated based on a design value of Z_1 using the following equations (Zhu et al., 2020):

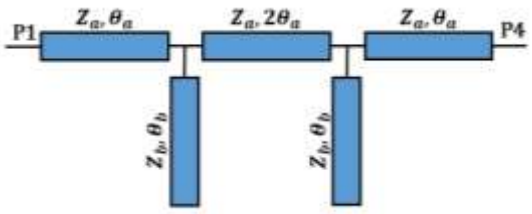

Figure 3. The schematic model of a dual-band phase inverter.

$$\theta_a = \frac{\pi}{1+n}, \qquad \theta_b = \frac{2\pi}{1+n}, \qquad n = \frac{f_2}{f_1} \tag{1}$$

$$Z_a = \frac{Z_1}{\tan\theta_a}, \qquad Z_b = \frac{Z_a \sin\theta_a \cos\theta_a \tan\theta_b}{\cos^2\theta_a - \sin^2\theta_a} \tag{2}$$

Figure 4 shows the effects of the frequency ratio (n) on the values of inverter`s transmission line impedances (Z_a & Z_b). The analysis shows that with the increase of frequency ratio (n), higher values of line impedances are required. The inverter's line impedances are also increasing with the increase of the original line impedance (Z_1).

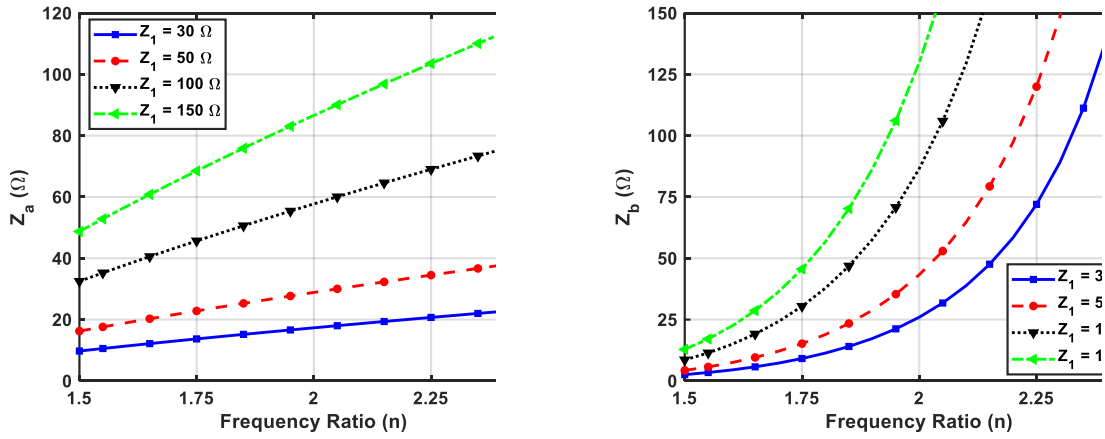

(a) (b)

Figure 4. Inverter`s transmission line impedances (Z_a and Z_b) versus the frequency ratio (n) with different values of line impedance Z_1. (a) Z_a vs. n (b) Z_b vs. n

The Proposed Dual-Band Balanced to Unbalanced Gysel Power Divider

The schematic of the proposed wideband dual-band balanced to unbalanced (BTU) Gysel power divider is shown in Fig. 5 after inserting the dual-band phase inverter. The divider is now a 4-port network with ports 1 and 4 as a differential input, and ports 2 and 3 as output ports. The divider consists of a dual-band phase inverter, three coupled line sections, two directly grounded isolation resistors (R), and a stepped-impedance stub on the right side. The stepped-impedance stub is used instead of just the open stub to maintain the output matching and

isolation. All the ports are 50 Ω.

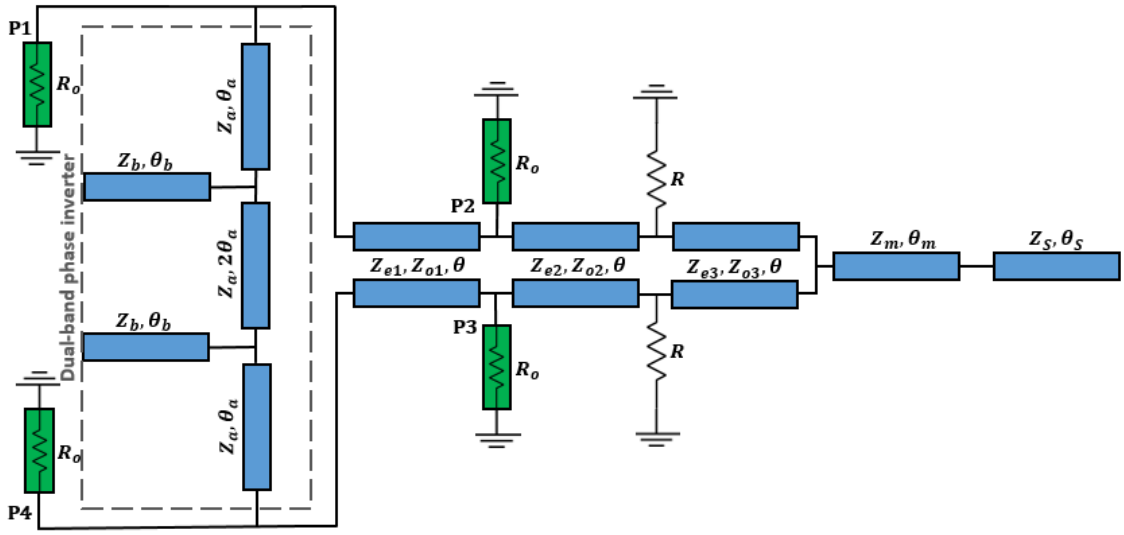

Figure 5. The schematic of a dual-band balanced to unbalanced (BTU) Gysel power divider.

Even and Odd Mode Analysis

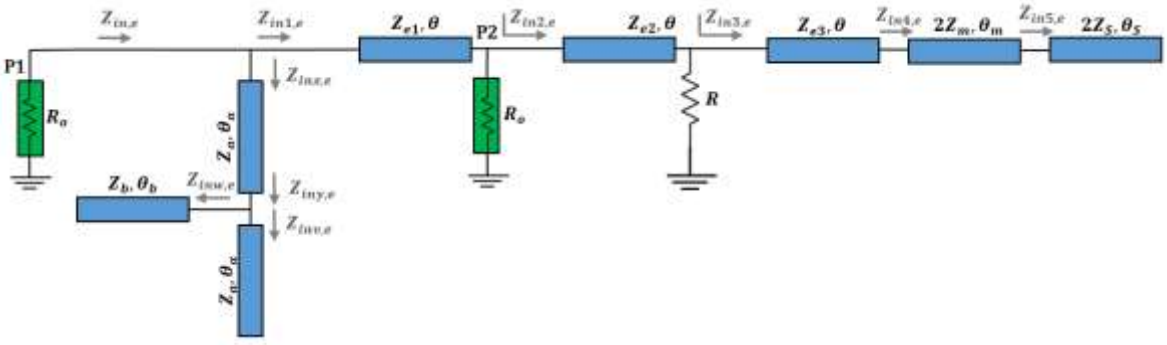

Figure 6. The schematic of the even-mode half circuit.

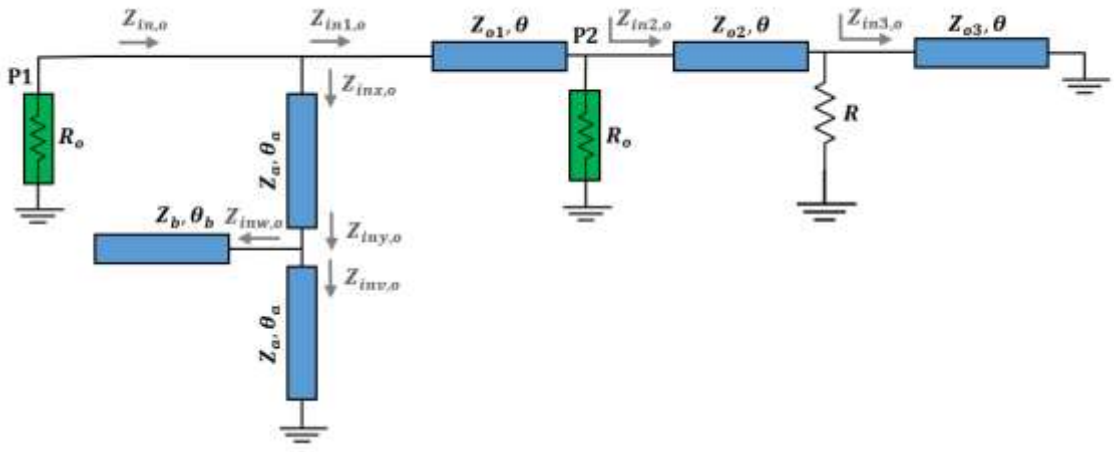

Figure 7. The schematic of the odd-mode half circuit.

The proposed structure is analyzed using even and odd mode analysis. The divider is simplified into two half equivalent circuits as shown in Figs. 6 and 7, by separating the even and odd mode characteristic impedances of the coupled line.

Even Mode Analysis

In the even-mode half (Fig. 6), the isolation resistor (R) has no current or voltage since the power divider must be matched at the two ports with lossless transmission. Therefore, the resistor (R) in Fig. 6 must be bypassed to the ground.

The input impedance seen at port 1 ($Z_{in,e}$) is derived as follows,

$$Z_{in5,e} = \frac{2Z_s}{j\tan\theta_s} \quad \textbf{(3)}$$

$$Z_{in4,e} = 2Z_m \frac{Z_{in5,e} + j\,2Z_m \tan\theta_m}{2Z_m + j\,Z_{in5,e}\tan\theta_m} \quad \textbf{(4)}$$

$$Z_{in3,e} = Z_{e3} \frac{Z_{in4,e} + j\,Z_{e3}\tan\theta}{Z_{e3} + j\,Z_{in4,e}\tan\theta} \quad \textbf{(5)}$$

Since the power divider must be matched at all ports and the power must be divided equally into the output ports at the two operating frequencies without any losses, the even-mode half circuit must be matched at both ports without any losses. As a results, the input impedance ($Z_{in3,e}$) must equal to zero and shorten the isolation resistor which removes its effects in this mode. Based on that, if $\theta_s = \theta_m = \theta$, the characteristic impedance (Z_{e3}) can be calculated as

$$Z_{e3} = 2Z_m \frac{[Z_m - Z_s(\tan\theta)^{-2}]}{[Z_m + Z_s]} \quad \textbf{(6)}$$

The impedance seen at port 2 ($Z_{in2,e}$) is now a parallel combination of the short stub (Z_{e2}, θ) with port 2 internal impedance (R_o),

$$Z_{in2,e} = R_o \parallel j\,Z_{e2}\tan\theta = \frac{j\,R_o\,Z_{e2}\tan\theta}{j\,Z_{e2}\tan\theta + R_o} \quad \textbf{(7)}$$

And from ($Z_{in2,e}$), the impedance ($Z_{in1,e}$) can be calculated by

$$Z_{in1,e} = Z_{e1} \frac{Z_{in2,e} + j\,Z_{e1}\tan\theta}{Z_{e1} + j\,Z_{in2,e}\tan\theta} \quad \textbf{(8)}$$

In the inverter circuit,

$$Z_{iny,e} = Z_{inv,e} \parallel Z_{inw,e} = \frac{Z_a}{j\tan\theta_a} \parallel \frac{Z_b}{j\tan\theta_b} = \frac{Z_a Z_b}{j\,[Z_a\tan\theta_b + Z_b\tan\theta_a]} \quad \textbf{(9)}$$

Then,

$$Z_{inx,e} = Z_a \frac{Z_{iny,e} + j\, Z_a \tan\theta}{Z_a + j\, Z_{iny,e} \tan\theta} \quad \textbf{(10)}$$

From Equations (8) and (10), the input impedance seen at port 1 ($Z_{in,e}$) is

$$Z_{in,e} = Z_{inx,e} \parallel Z_{in1,e} = \frac{Z_{in1,e}\, Z_{inx,e}}{Z_{in1,e} + Z_{inx,e}} \quad \textbf{(11)}$$

In addition, the ABCD matrix of the even mode excitation, from port 1 to port 2 can be obtained as follows:

$$\begin{bmatrix} A_e & B_e \\ C_e & D_e \end{bmatrix} = \begin{bmatrix} 1 & 0 \\ \frac{1}{Z_{inx,e}} & 1 \end{bmatrix} \begin{bmatrix} \cos\theta & jZ_{e1}\sin\theta \\ \frac{\mathrm{j}\sin\theta}{Z_{e1}} & \cos\theta \end{bmatrix} \begin{bmatrix} 1 & 0 \\ \frac{1}{Z_{in2,e}} & 1 \end{bmatrix} \quad \textbf{(12)}$$

Odd Mode Analysis

The odd-mode half circuit is shown in Fig. 7, where the inverter circuit and open stub line are now bypass to the ground. The input impedance seen at port 1 (Z_{in}) is derived as follows,

$$Z_{in3,o} = j\, \mathrm{Z_{o3}} \tan\theta \quad \textbf{(13)}$$

and

$$Z_{in2,o} = Z_{o2} \frac{Z_2 + j\, Z_{o2} \tan\theta}{Z_{o2} + j\, Z_2 \tan\theta} \quad \textbf{(14)}$$

Where Z_2 is defined as

$$Z_2 = R \parallel j\, Z_{e3} \tan\theta = \frac{j\, R\, Z_{o3} \tan\theta}{j\, Z_{o3} \tan\theta + R} \quad \textbf{(15)}$$

Also,

$$Z_{in1,o} = Z_{o1} \frac{Z_4 + j\, Z_{o1} \tan\theta}{Z_{o1} + j\, Z_4 \tan\theta} \quad \textbf{(16)}$$

Where Z_4 is defined as

$$Z_4 = Z_{in2,o} \parallel R_o = \frac{Z_{in2,o}\, R_o}{Z_{in2,o} + R_o} \quad \textbf{(17)}$$

In the inverter circuit,

$$Z_{iny,o} = Z_{inv,o} \parallel Z_{inw,o} = j\, Z_a \tan\theta_a \parallel \frac{Z_b}{j \tan\theta_b} = \frac{Z_a Z_b}{j\,[Z_a \tan\theta_b - Z_b \tan\theta_a]} \quad \textbf{(18)}$$

Then,

$$Z_{inx,o} = Z_a \frac{Z_{iny,o} + j\, Z_a \tan\theta}{Z_a + j\, Z_{iny,o} \tan\theta} \quad \textbf{(19)}$$

From Equations (16) and (19), the input impedance seen at port 1 ($Z_{in,o}$) is

$$Z_{in,o} = Z_{in1,o} \parallel Z_{inx,o} = \frac{Z_{in1,o}\, Z_{inx,o}}{Z_{in1,o} + Z_{inx,o}} \quad \textbf{(20)}$$

The ABCD matrix of the odd mode excitation, from port 1 to port 2 can be obtained as follows:

$$\begin{bmatrix} A_o & B_o \\ C_o & D_o \end{bmatrix} = \begin{bmatrix} 1 & 0 \\ \frac{1}{Z_{inx,o}} & 1 \end{bmatrix} \begin{bmatrix} \cos\theta & jZ_{o1}\sin\theta \\ \frac{\mathrm{j}\sin\theta}{Z_{o1}} & \cos\theta \end{bmatrix} \begin{bmatrix} 1 & 0 \\ \frac{1}{Z_{in2,o}} & 1 \end{bmatrix} \quad \textbf{(21)}$$

S-Parameters of the Proposed Device

To evaluate the performance of the proposed BTU Gysel power divider, the standard scattering matric $[S^{SE}]$ of the proposed design are obtained as follow

$$[S^{SE}] = \begin{bmatrix} -\frac{1}{2} & S_{21} & S_{31} & -\frac{1}{2} \\ S_{21} & 0 & 0 & -S_{21} \\ S_{31} & 0 & 0 & -S_{31} \\ -\frac{1}{2} & -S_{21} & -S_{31} & -\frac{1}{2} \end{bmatrix} \quad \textbf{(22)}$$

The above matrix is derived to obtain perfect input matching at all ports and perfect isolation between output ports and they can be calculated from the ABCD matrices of the even and odd circuits (Equations (12) and (21)). Based on the standard S-parameters in Equation (22), The mixed mode scattering matrix $[S^{MM}]$ is derived as

$$[S^{MM}] = \begin{bmatrix} S_{d1d1} & S_{d1s2} & S_{d1s3} & S_{d1c1} \\ S_{s2d1} & S_{s2s2} & S_{s2s3} & S_{s2c1} \\ S_{s3d1} & S_{s3s2} & S_{s3s3} & S_{s3c1} \\ S_{c1d1} & S_{c1s2} & S_{c1s3} & S_{c1c1} \end{bmatrix} = \begin{bmatrix} 0 & \sqrt{2}S_{21} & \sqrt{2}S_{31} & 0 \\ \sqrt{2}S_{21} & 0 & 0 & 0 \\ \sqrt{2}S_{31} & 0 & 0 & 0 \\ 0 & 0 & 0 & -1 \end{bmatrix} \quad \textbf{(23)}$$

The above matrix has the following targets: (a) perfect input matching at all ports, (b) equal power division from port 1 into ports 2 and 3, (c) perfect isolation between output ports (2 and 3), (d) perfect common mode rejection at port 1, (e) no common mode transmission from port 1 into ports 2 and 3. For dual-band operation, the center frequencies are f_1 and $f_2 = nf_1$, where n ≥ 1, and the simplest condition for electrical length is represented as:

$$\theta_{f1} = \frac{\pi}{1+n}, \qquad \theta_{f2} = \frac{n\pi}{1+n} \quad \textbf{(24)}$$

Parametric Studies

Equation (6) shows that there are two degrees of freedom to choose the design parameters (Z_s, Z_m, and Z_{e3}). Fig. 8a shows the effects of the frequency ratio (n) on the transmission line impedance (Z_{e3}) with line impedance ($Z_m = 100\ \Omega$) and different values of the line impedance (Z_s). In general, the transmission line impedance (Z_{e3}) decreases with the increase of (n) but it was decreasing faster with the increase of the line impedance (Z_s).

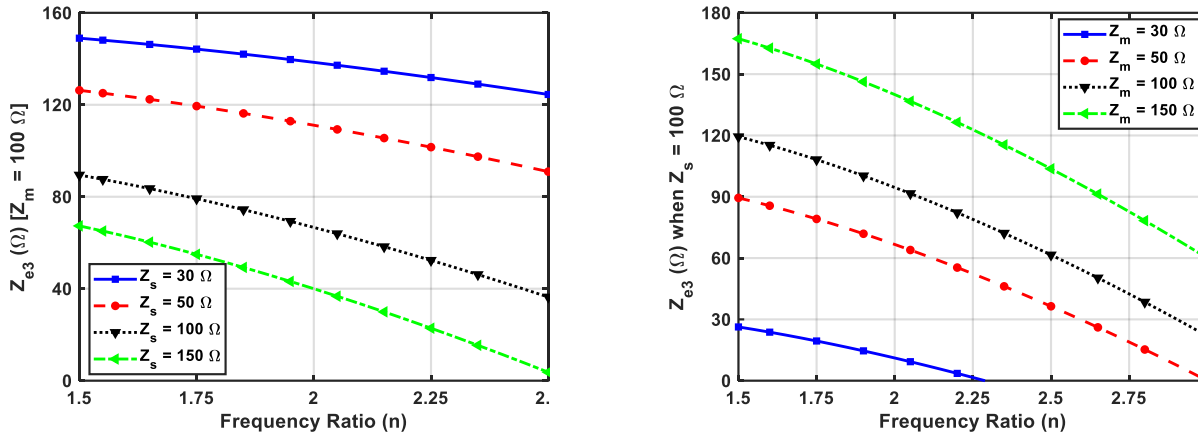

(a) (b)

Figure 8. Transmission line impedance (Z_{e3}) versus the frequency ratio (n). (a) with line impedance ($Z_m = 100\ \Omega$) and different values of line impedance (Z_s). (b) with line impedance ($Z_s = 100\ \Omega$) and different values of line impedance (Z_m) .

Fig. 8b shows the effects of the frequency ratio (n) on the transmission line impedance (Z_{e3}) with line impedance ($Z_s = 100\ \Omega$) and different values of the line impedance (Z_m). In general, the transmission line impedance (Z_{e3}) decreases with the increase of (n) but it was increasing faster with the increase of the line impedance (Z_m).

RESULTS AND DISCUSSION

A wideband dual-band BTU power Gysel power divider is implemented at two operating frequencies (2.4 and 5 GHz) which results in $n = 2.083$. The implementation starts when $\theta = \theta_{f1}$ is equal to 58.4° which is calculated from Equation (24), the design parameters (Z_S, Z_m, and Z_{e3}) are designed using Equation (6). The following parameters (Z_a, Z_b, Z_{e1}, Z_{o1}, Z_{e2}, Z_{o2}, Z_{o3}, and R) can be designed using the above equations with large area of freedom.

In order to implement the transmission lines, their characteristic impedances are chosen to be between 30 Ω and 150 Ω, which are reasonable to manufacture using standard etching machine, and with considering the mixed mode scattering matrix of the proposed design, the design parameters are: $Z_a = 54\ \Omega$, $Z_b = 115\ \Omega$, $Z_{e1} = 115.5\ \Omega$, $Z_{o1} = 48.5\ \Omega$, $Z_{e2} = 70\ \Omega$, $Z_{o2} = 65\ \Omega$, $Z_{e3} = 108\ \Omega$, $Z_{o3} = 30\ \Omega$, $Z_m = 140\ \Omega$, $Z_S = 90\ \Omega$, $R = 110\ \Omega$, $\theta = \theta_s = \theta_m = \theta_a = 58.4^o$, and $\theta_b = 116.8^o$. The mixed mode S-parameters of the proposed power dividers are shown in Figs. 9-12.

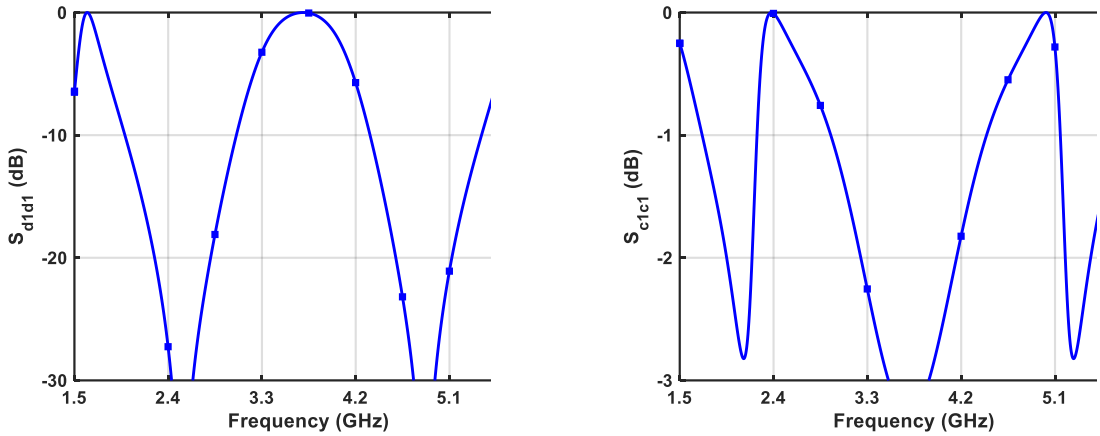

(a) (b)

Figure 9. (a) The differential mode input return loss $|S_{d1d1}|$ versus frequency. (b) The common mode input return loss $|S_{c1c1}|$ versus frequency.

Fig. 9a shows that the differential mode signal going into the differential input port (input return loss at port 1) is perfectly matched at the desired frequencies, where $|S_{d1d1}|$ = -27.25 dB at 2.4 GHz with a 10-dB bandwidth of 45.83% (1100 MHz) and $|S_{d1d1}|$ = -26.39 dB at 5 GHz with a 10-dB bandwidth of 21.4% (1070 MHz). Fig. 9b shows that the common mode noise going into the differential port (port 1) is totally reflected where $|S_{c1c1}|$ = 0 dB at both 2.4 GHz and 5 GHz. In Fig. 10, the differential/balanced signal from port 1 is transmitted into the two single output ports (port 2 and 3) with equal power division where, $|S_{s2d1}| = |S_{s3d1}| = |S_{d1s2}| = |S_{d1s3}|$ = -3.33 dB at 2.4 GHz with a 3-dB bandwidth of 61.37% (1473 MHz), and -3.34 dB at 5 GHz with a 3-dB bandwidth of 29.42% (1471 MHz). The proposed device has a wideband power division performance which makes it a great candidate for wideband applications.

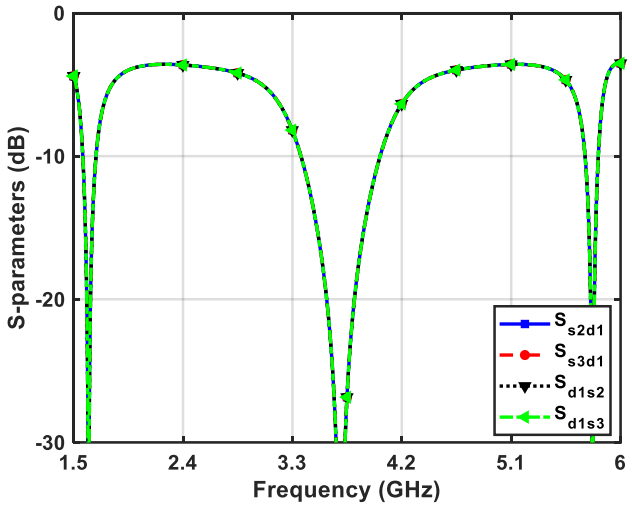

Figure 10. The output power division parameters ($|S_{s2d1}| = |S_{s3d1}| = |S_{d1s2}| = |S_{d1s3}|$) versus frequency.

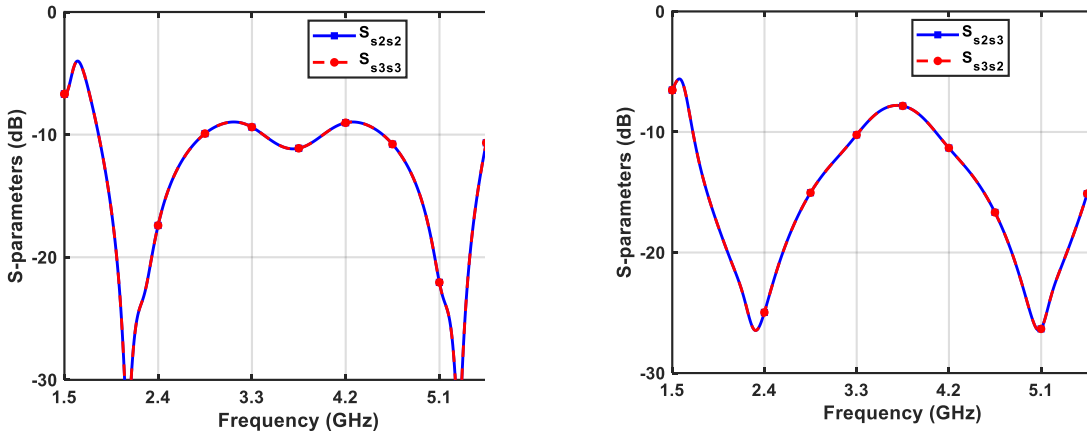

(a) (b)

Figure 11. (a) Output return loss S-parameters at ports 2 and 3 ($|S_{s2s2}| = |S_{s3s3}|$) vs. frequency. (b) Isolation S-parameters between the output ports ($|S_{s2s3}| = |S_{s3s2}|$) vs. frequency.

Fig. 11a shows that the output return loss S-parameters at ports 2 and 3 ($|S_{s2s2}| = |S_{s3s3}|$) are equal to -17.41 dB at 2.4 GHz and -18.01 dB at 5 GHz which results in a good matching at these ports. The isolation S-parameters between the output ports ($|S_{s2s3}| = |S_{s3s2}|$) were perfect with -24.97 at 2.4 GHz and-25.39 at 5 GHz as shown in Fig. 11b. Fig. 12 shows a perfect common mode suppression as there is no power converted to the common mode with $|S_{c1s2}| = |S_{c1s3}| = |S_{s2c1}| = |S_{s3c1}|$ = -34.61 dB at 2.4 GHz and -47.49 dB at 5 GHz.

A summary of the simulated mixed-mode S-parameters results are shown in Table 1 at the operating frequencies (2.4 GHz & 5 GHz). The results are found using Keysight-ADS and show a great power divider performance. Moreover, the result was verified, and the exact same results were found using the ABCD matrix by MATLAB.

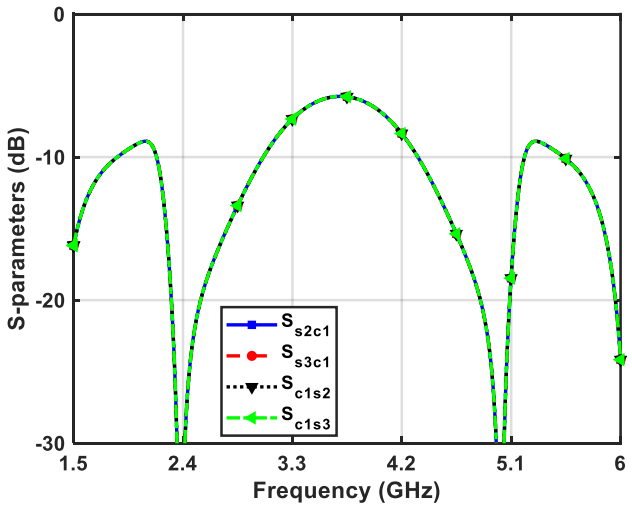

Figure 12. The common mode S-parameters ($|S_{s2c1}|$, $|S_{s3c1}|$, $|S_{c1s2}|$, and $|S_{c1s3}|$) versus frequency.

Table 1. The simulated S-parameters of the proposed design at the operating frequencies.

	S-Parameters at 2.4 GHz (dB)	S-Parameters at 5 GHz (dB)
S_{d1d1}	-27.25	-26.39
$S_{d1s2} = S_{d1s3}$	-3.33	-3.34
$S_{s2d1} = S_{s3d1}$	-3.33	-3.37
$S_{c1d1} = S_{d1c1}$	-300	-300
S_{s2s2}	-17.41	-18.01
$S_{s2s3} = S_{s3s2}$	-24.97	-25.39
S_{s3s3}	-17.41	-18.01
$S_{c1s2} = S_{c1s3} = S_{s2c1} = S_{s3c1}$	-34.61	-47.49
S_{c1c1}	0	0

Table 2. Comparison between the performance of the proposed divider and similar existing devices.

Parameter	Zhu et al., 2020	Zhuang et al., 2018	This Work
f_1 & f_2 in GHz	1 & 2	1 & 6.4	2.4 & 5
S_{d1d1} (at f_1 & f_2) in dB	-27.1 & -24.1	-27 & -28	-27.25 & -26.39
S_{s2s3} (at f_1 & f_2) in dB	-21.9 & -16.3	-22 & -14	-24.97 & -25.39
$S_{c1s2} = S_{c1s3} = S_{s2c1} = S_{s3c1}$ (at f_1 & f_2) in dB	-36.3 & -28.4	-38.3 & -28.2	-34.61 & -47.49

In Table 2, the performance of the proposed divider is compared to the results reported for the dividers presented in (Zhu et al., 2020; Zhuang et al., 2018). The comparison is conducted in terms of the differential return loss, the isolation between the output ports, and the common mode suppression. It can be seen that the proposed device offers a performance comparable to the existing device while providing improved output isolation. This asserts its suitability for applications requiring reliable performance.

CONCLUSIONS

A wideband dual-band balanced to unbalanced (BTU) Gysel power divider using coupled lines for dual-band WiFi applications is verified. The design of divider incorporates a dual-band phase inverter to implement the differential functionality at the input port, and stepped-impedance stub was added to improve the output matching and isolation. The electrical design parameters and the ABCD matrix were derived from the even and odd mode analysis. The proposed theoretical derivation shows that the proposed device has many parameters that can be designed with high area of freedom. The parameters can be chosen to obtain a compact size and wideband response, and flexible design was achieved by using coupled lines. Moreover, the simulated results show a great performance at the operating frequencies (2.4 GHz and 5 GHz) in terms of wideband response, perfect common

mode suppression, and excellent output isolation.

REFERENCES

Wu, C. H., Wang, C. H., and Chen C. H. 2007. Novel balanced coupled-line bandpass filters with common-mode noise suppression. IEEE Trans. Microw. Theory Techn. 55(2): pp. 287–295.

Lim, J. E., Nam, M. H., Chon, H. O., and Lee, J. H. 2010. Two-port balanced dual-band bandpass filter based on stepped impedance resonators. Proc. Asia–Pacific Microw. Conf. pp. 1114–1117.

Jiao, L., Wu, Y., Zhang, W., Li, M., Liu, Y., Xue, Q., and Ghassemlooy, Z. 2018. Design methodology for six-port equal/unequal quadrature and rat-race couplers with balanced and unbalanced ports terminated by arbitrary resistances. IEEE Trans. Microw. Theory Techn. 66(3): pp. 1249–1262.

Li, L., Mao, J.-F., and Wu, L.-S. 2019. A single-ended-to-balanced impedance-transforming branch-line coupler with arbitrary power division ratio. IEEE Trans. Microw. Theory Techn. 67(3): pp. 949–956.

Lobato-Morales, H., Sun, J. S., Corona-Chavez, A., Itoh, T., and Olvera-Cervantes, J. L. 2012. UWB and WLAN microstrip diplexer for differential-mode operation. IEEE MTT-S Int. Microw. Symp. Dig. pp. 1–3.

Zhou, Y. G., Deng, H. W., and Zhao, Y. J. 2014. Compact balanced-to-balanced microstrip diplexer with high isolation and common-mode suppression. IEEE Microw. Wireless Compon. Lett. 24(3): pp. 143–145.

Sun, Z. Y., Zhang, L. J., Liu, Y.Z., and Tong, X. D. 2011. Modified Gysel Power Divider for Dual-Band Applications. *IEEE Microw. Wireless Compon. Lett.* 21(1): pp. 16-18.

Yoon, Y.-C. and Kim, Y. 2021. Unequal Power Dividers Using Uniform Impedance Transmission Lines with Stubs. J Electromagn. Eng Sci. 21(1): pp. 44–50.

Sun, Z., Zhang, L., and Yan, Y. 2011. A novel unequal dual-band Gysel power divider. IEEE MTT-S International Microwave Symposium, Baltimore, MD, USA. pp. 1–4.

Wang, X., Wu, K.-L., and Yin, W.-Y. 2014. A Compact Gysel Power Divider with Unequal Power-Dividing Ratio Using One Resistor. IEEE Trans. Microwave Theory Techn. 62(7): pp. 1480–1486.

Wang, W. M., Wu, Y. L., and Liu, Y. A. 2013. A Novel Coupled-Line Gysel Power Divider for Dual-Band and High-Power applications. AMR. (834–836): pp. 1132–1139.

Wang, W., Wu, Y., and Liu, Y. 2014. A Novel High-Power Dual-Band Coupled-Line Gysel Power Divider with Impedance-Transforming Functions. The Scientific World Journal. 2014: pp. 1–9.

Zhang, W. et al. 2017. Novel Planar Compact Coupled-Line Single-Ended-to-Balanced Power Divider. IEEE Trans. Microwave Theory Techn. 65(8): pp. 2953–2963.

Yu, Y. and Sun, L. 2015. A design of single-ended to differential-ended power divider for X band application. Microw. Opt. Technol. Lett. 57(11): pp. 2669–2673.

Wu, Y., Zhuang, Z., Kong, M., Jiao, L., Liu, Y., and Kishk, A. 2018. Wideband Filtering Unbalanced-to-Balanced Independent Impedance-Transforming Power Divider with Arbitrary Power Ratio. IEEE Trans. Microwave Theory Techn. 66(10): pp. 4482–4496.

Feng, W., Wang, C., Shi, Y., Gómez-García, R., and Che, W. 2019. Compact dual-band single-ended-to-balanced power dividers with open/short-ended stubs. Int J RF Microw Comput Aided Eng. 29(7): p. e21812.

Xu, k., Shi, J., Lin, L., and Chen, J.-X. 2015. A Balanced-to-Unbalanced Microstrip Power Divider with Filtering Function. IEEE Trans. Microwave Theory Techn. 63(8): pp. 2561–2569.

Zhu, Z., Wang, Z., Ma, J., Liu, H., and Fang, S. 2020. Dual-Band Balanced-to-Unbalanced Power Divider with

Independent Power Division Ratios. IEEE Access. 8: pp. 192659–192668.

Wu, L.-S., Guo, Y.-X., and Mao, J.-F. 2013. Balanced-to-Balanced Gysel Power Divider with Bandpass Filtering Response. IEEE Trans. Microwave Theory Techn. 61(12): pp. 4052–4062.

Xia, B., Wu, L.-S., and Mao, J. 2012. A New Balanced-to-Balanced Power Divider/Combiner. IEEE Trans. Microwave Theory Techn. 60(9): pp. 2791–2798.

Li, M., Wu, Y., Jiao, L., Ma, L., Wang, W., and Liu, Y. 2018. A planar balanced-to-balanced power divider with wideband filtering responses and common-mode suppressions. IEEE Access. 6: pp. 42057–42065.

Zhuang, Z., Wu, Y., Kong, M., Wang, W. and Liu, Y. 2018. Dual-Band Filtering Balanced-to-Unbalanced Impedance-Transforming Power Divider with High Frequency Ratio and Arbitrary Power Division. IEEE Access. 6: pp. 12710-12717.

Liu, Z., Zhang, Q., Guo, Z., et al. 2022. A novel dual-band balanced-to-single-ended in-phase filtering power divider based on slotted circular patch resonator. Int J RF Microw Comput Aided Eng. 32(9): e23274.

Alazemi, A., Kourah, M. 2019. Equal and unequal quad-band Gysel power dividers. *Int J RF Microw Comput Aided Eng*. 29: e21635.